Energy & Environmental Science

COMMUNICATION

Discovering Ce-rich oxygen evolution catalysts, from high throughput screening to water electrolysis†

Cite this: *Energy Environ. Sci.*, 2014, 7, 682

Received 9th November 2013
Accepted 3rd January 2014

DOI: 10.1039/c3ee43683g

www.rsc.org/ees

Joel A. Haber,[a] Yun Cai,[b] Suho Jung,[a] Chengxiang Xiang,[a] Slobodan Mitrovic,[a] Jian Jin,[ac] Alexis T. Bell[bd] and John M. Gregoire*[a]

We report a new Ce-rich family of active oxygen evolution reaction (OER) catalysts composed of earth abundant elements, discovered using high-throughput methods. High resolution inkjet printing was used to produce 5456 discrete oxide compositions containing the elements nickel, iron, cobalt and cerium. The catalytic performance of each of these compositions was measured under conditions applicable to distributed solar fuels generation using a three-electrode scanning drop electrochemical cell. The catalytic activity and stability of representative compositions ($Ni_{0.5}Fe_{0.3}Co_{0.17}Ce_{0.03}O_x$ and $Ni_{0.3}Fe_{0.07}Co_{0.2}Ce_{0.43}O_x$) from 2 distinct regions were verified by resynthesizing these compositions on glassy carbon rods for electrochemical testing. The activity of the new Ce-rich catalysts was further verified using an unrelated synthetic method to electrodeposit a pseudo-ternary composition $Ni_{0.2}Co_{0.3}Ce_{0.5}O_x$, which produced a catalyst with 10 mA cm^{-2} oxygen evolution current at 310 mV overpotential. The unique Tafel behavior of these Ce-rich catalysts affords the opportunity for further improvement.

Broader context

The development of new, environmentally friendly energy technologies critically depends upon the discovery and development of new functional materials. For example, efficient conversion of solar energy to fuels requires the discovery of new electrocatalysts, particularly for the oxygen evolution reaction (OER). Large-scale deployment of this type of system requires the discovery of improved electrocatalysts containing only earth-abundant elements. Lacking a robust fundamental understanding of the basic science and mechanistic details of multi-electron heterogeneous electrocatalysis, an efficient high-throughput synthesis and property screening methodology is well-suited to discovering the requisite new catalytic materials. The effectiveness of this approach is demonstrated by our discovery of a new, highly active OER catalyst in an unpredicted composition space, displaying unusual electrochemical behavior. We describe high throughput synthesis, screening techniques and figures of merit designed specifically for discovery of OER catalysts for artificial photosynthesis.

The efficient electrochemical conversion of H_2O and CO_2 into fuel is an attractive technique for storing energy produced by intermittent renewable energy sources such as solar or wind. Feasible large-scale deployment of this type of system requires the discovery of improved electrocatalysts containing only earth-abundant elements.[1–3] In particular, the 4-electron oxygen evolution reaction (OER) is kinetically slow and improved catalysts are required for artificial photosynthesis and electrolysis of hydrogen or carbon-containing fuels.[2] Because a robust fundamental understanding of the basic science and mechanistic details of multi-electron heterogeneous electrocatalysis is lacking, an efficient high-throughput synthesis and property screening methodology is well-suited to empirically discovering the requisite new catalytic materials.[4–11] Ideally, the newly discovered materials will not only perform better under operational conditions, but display unique behaviors that contribute to the fundamental understanding of these complex reactions. Combinatorial methods have previously been used to search pseudoternary spaces for improved OER catalysts.[7–9] To broaden the catalyst search we have developed very high throughput techniques capable of screening pseudoquaternary spaces and describe high throughput screening techniques designed specifically for discovery of OER catalysts for artificial photosynthesis. The effectiveness of this approach is demonstrated by our discovery of a new, highly active family of OER catalysts in an unpredicted composition space, providing new pathways for engineering optimization and OER catalysis science.

Mixed metal oxides in the $(Ni–Fe)O_x$ and $(Ni–Co)O_x$ composition spaces are among the most active and most studied OER

[a]Joint Center for Artificial Photosynthesis, California Institute of Technology, Pasadena, California 91125, USA. E-mail: gregoire@caltech.edu
[b]Joint Center for Artificial Photosynthesis, Lawrence Berkeley National Laboratory, Berkeley, California 94720, USA
[c]Engineering Division, Lawrence Berkeley National Laboratory, Berkeley, California 94720, USA
[d]Department of Chemical and Biomolecular Engineering, University of California at Berkeley, Berkeley, California 94720, USA

† Electronic supplementary information (ESI) available: Experimental details, additional electrochemical data, SEM micrographs, XRD, XPS, testbed electrolyzer data, comparison of intended library compositions to EDS compositions. See DOI: 10.1039/c3ee43683g

catalysts.[2,12–19] The addition of a few at% Ce to Ni has also been reported to provide an initial enhancement in activity.[20] However, over time that activity degrades to overpotentials typical for Ni-based catalysts.[21] To identify the optimal Ni-based mixed metal composition with Ce addition, we have used a high-throughput strategy to synthesize all compositions at 3.3 at% steps in the pseudoquaternary (Ni–Fe–Co–Ce)O_x composition space. In contrast to a more traditional approach of modifying a known high-performing material to find a locally optimal composition,[5] our thorough investigation of the entire pseudoquaternary phase space revealed a new catalytically active composition region, separated from the known (Ni–Fe)O_x region by less active compositions. High throughput measurement conditions are often quite different from technologically relevant conditions, inhibiting direct transfer of hit materials to operational devices. To address this challenge, we rapidly executed follow-up studies to accelerate the technological development of the newly discovered material. Catalysts in this previously unexplored composition space were evaluated using several standard electrochemical techniques, resynthesized using an alternate deposition technique, and operated in a solar fuels testbed system. These studies verified the performance and viability of the catalyst and additionally revealed a unique Tafel behavior, providing opportunities for further scientific study and engineering optimization.

The pseudo-quaternary (Ni–Fe–Co–Ce)O_x library was deposited as an array of 5456 discrete compositions at 3.3 at% composition steps.[22,23] The compositions were produced by inkjet printing four separate metal precursor inks (3.8 nanomoles of metal in each 1 mm^2 spot), prepared by a previously described method,[11,24] onto a conducting substrate. The inks were dried and the metal precursors converted to oxides by calcination in air at 350 °C. This produced material that was X-ray amorphous, which has been shown to improve the performance of some OER catalysts.[25,26] Multiple spots in the library were confirmed by EDX to have the intended compositions. The catalytic performance of each composition was evaluated in O_2-saturated 1.0 M NaOH(aq) using a previously described, custom-built scanning droplet cell (SDC).[23] The scanning droplet cell provided an individual 3-electrode cell for each sample, including the conducting substrate, a capillary Ag/AgCl reference electrode and a platinum wire counter electrode. The activity of each catalyst composition was characterized using a 10 s chronopotentiometry (CP) measurement at 10 mA cm^{-2} (geometric area, all current densities in this work reference geometric area), followed by a cyclic voltammetry (CV) measurement between 0 mV and 440 mV overpotential for the OER reaction with a sweep rate of 150 mV s^{-1}. Further details are available in the ESI.†

The relative electrocatalytic performance of each composition was screened using several different figures of merit (FOM). A 10% efficient artificial photosynthetic system produces a catalytic current of approximately 10 mA cm^{-2} (geometric area);[1] therefore, the most informative FOM for photoelectrochemical water-splitting devices is the overpotential (η) for the OER at 10 mA cm^{-2},[21,27,28] which is mapped in Fig. 1 for the entire composition space. In Fig. 1A, the most active regions can be seen near the Ni–Fe edge and on the Ni–Co–Ce face of the tetrahedron. To visualize the full quaternary map of η, Fig. 1B represents the data as a series of slices through the tetrahedral composition space, parallel to the triangular Ni–Fe–Co base. Plotting the catalytic activity from our library of closely spaced discreet composition spots clearly shows that activity varies smoothly with composition, and thus we define catalyst composition regions and choose representative specific compositions from those regions. The pseudoternary slice containing the $Ce_{0–0.09}$ composition range shows that slight improvements to the known (Ni–Fe)O_x catalyst are attained in nearby compositions with the locally optimal catalyst at composition $Ni_{0.5}Fe_{0.3}Co_{0.17}Ce_{0.03}O_x$, hereafter referred to as the *low-Ce* catalyst. Comparable overpotential is attained in a previously unexplored composition region shown in the $Ce_{0.40–0.49}$ pseudoternary plot with locally optimal composition $Ni_{0.3}Fe_{0.07}Co_{0.2}Ce_{0.43}O_x$, hereafter referred to as the *high-Ce* catalyst.

To better visualize the activity trend between and around these locally optimal compositions, a pseudoternary slice depicted in Fig. 2A is shown in Fig. 2B. This visualization of the relationship between the two catalysts provides a clear depiction of why a traditional gradient-based search algorithm would fail to identify the new *high-Ce* catalyst. A more traditional search strategy would start with a known performer and modify it to identify trends in improved performance that lead to a superior composition. Our high throughput screening demonstrates that applying this methodology to the known highly

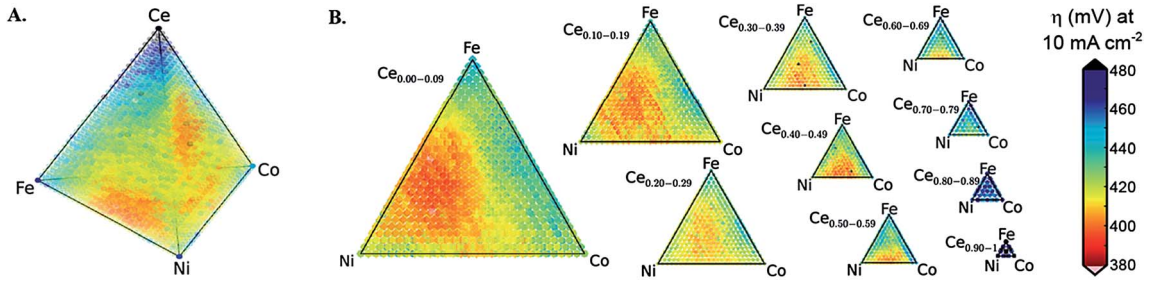

Fig. 1 Performance map of (Ni–Fe–Co–Ce)O_x oxygen evolution catalysts. The composition map of the overpotential required for performing oxygen evolution at 10 mA cm^{-2} from CP measurements is shown (A) in the quaternary composition tetrahedron and (B) as a series of pseudoternary slices through the quaternary space.

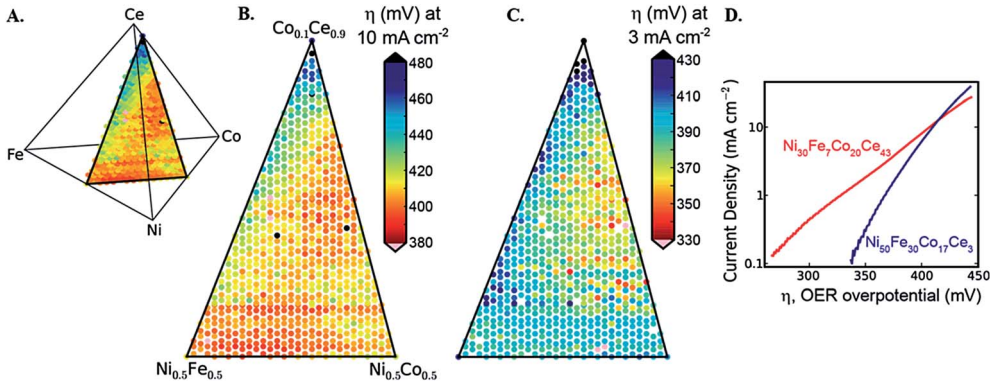

Fig. 2 Analysis of a pseudoternary section of the (Ni–Fe–Co–Ce)O_x catalyst space. (A) A planar slice through the tetrahedron of Fig. 1B that intersects the composition regions of interest. The pseudoternary map of the planar slice showing the overpotential (B) at 10 mA cm^{-2} as in Fig. 1 and (C) at 3 mA cm^{-2} from CV data. (D) The catalytic current extracted from CV measurements is shown for the representative high-Ce and low-Ce catalysts.

active (Ni–Fe)O_x by addition of Ce and Co additives would lead to identification of an optimal composition near $Ni_{0.5}Fe_{0.3}Co_{0.17}Ce_{0.03}O_x$, at which point the search would terminate. Due to the local minima in performance between the two highly active catalyst composition regions, the identification of $Ni_{0.3}Fe_{0.07}Co_{0.2}Ce_{0.43}O_x$ requires a broader search strategy.

Since optimized catalyst electrodes can typically be synthesized with an electrochemically active surface area many times greater than the geometric surface area, lower geometric current densities are also relevant to FOM catalyst screens for artificial photosynthesis, motivating our definition of a second FOM, the OER catalyst overpotential at 3 mA cm^{-2}. Fig. 2C presents this alternative FOM, showing that at this lower current density the newly discovered *high-Ce* catalyst requires significantly lower overpotential than the *low-Ce* compositions.

While the high-throughput synthesis and screening techniques described above enabled the discovery of a new OER catalyst, we used traditional electrochemical techniques to confirm the catalytic activity. The representative compositions from the *low-Ce* and *high-Ce* composition regions were deposited on glassy carbon (GC) rods (at 7.5 nanomoles of metal per mm^2) using the same inkjet printing and processing conditions used to prepare the composition library on FTO-coated glass plates. The GC rods coated with each composition were used as rotating disk electrodes (RDE) and subjected to a standardized series of electrochemical characterizations specifically designed for evaluating the activity and stability of electrocatalysts for solar water splitting devices, described in detail elsewhere,[21] and in the ESI. In brief, each electrode was analyzed in O_2-saturated 1.0 M NaOH blanketed under 1 atm $O_2(g)$. A sequence of electrochemical measurements was performed including CVs, electrochemical surface area measurements, several 30 s CP step and chronoamperometry (CA) step measurements and a 2 h CP measurement at 10 mA cm^{-2} to evaluate catalyst stability.

To ensure that the catalytic activity from the *high-Ce* composition region is not reliant on the ink-based deposition technique, electrodeposition was used to synthesize a catalyst in the pseudoternary (Ni–Co–Ce)O_x composition space (specifically, $Ni_{0.2}Co_{0.3}Ce_{0.5}O_x$). The pseudoternary composition was targeted for synthesis instead of the pseudoquaternary composition prepared by ink-jet printing, because the three-metal film composition is more readily prepared *via* electrodeposition. Moreover, inspection of the activity (overpotential at 10 mA cm^{-2}) of the relevant compositions in the catalyst libraries in Fig. 1 and 2 indicates no significant difference in activity between these two compositions. That is, $Ni_{0.3}Fe_{0.07}Co_{0.2}Ce_{0.43}O_x$ is at the center of the *high-Ce* composition range of high activity (and therefore the composition targeted by IJP), but the stoichiometrically simpler $Ni_{0.2}Co_{0.3}Ce_{0.5}O_x$ composition is in the same composition region and essentially identical in activity. The $Ni_{0.2}Co_{0.3}Ce_{0.5}O_x$ catalyst film was electrodeposited onto a smooth Au RDE electrode from a N_2-saturated mixed metal nitrate solution. The catalyst performance was evaluated with the electrode rotated at 1600 rpm in an O_2-saturated 1.0 M NaOH aqueous solution. The OER activity of the catalyst was investigated with six CV cycles at 10 mV s^{-1} (see ESI†) followed by a series of stepped 90 second CP (30, 10, 3, 1, 0.3 mA cm^{-2} geometric area) measurements.

Fig. 3 summarizes the electrochemical characterization of the two compositions of interest, combining data from the combinatorial library catalysts, inkjet-deposited RDE catalysts, and electrodeposited catalysts. Comparing the SDC and RDE measurements, the two compositions have similar relative performance, with higher catalytic currents obtained in the RDE experiments. For the *high-Ce* composition, even larger currents were observed with the electrodeposited sample. At 10 mA cm^{-2}, the overpotential from the SDC and RDE measurements on inkjet-deposited samples were 410 mV and 370 mV, respectively. The corresponding value for the electrodeposited sample was 310 mV, among the lowest reported for OER catalysts.

For each composition, the different samples and measurement techniques produced a consistent voltage-dependence of the catalytic current, which is typically quantified by the Tafel slope. The quasi-steady state RDE CP and RDE CA measurements provide the best data for determination of Tafel slope.

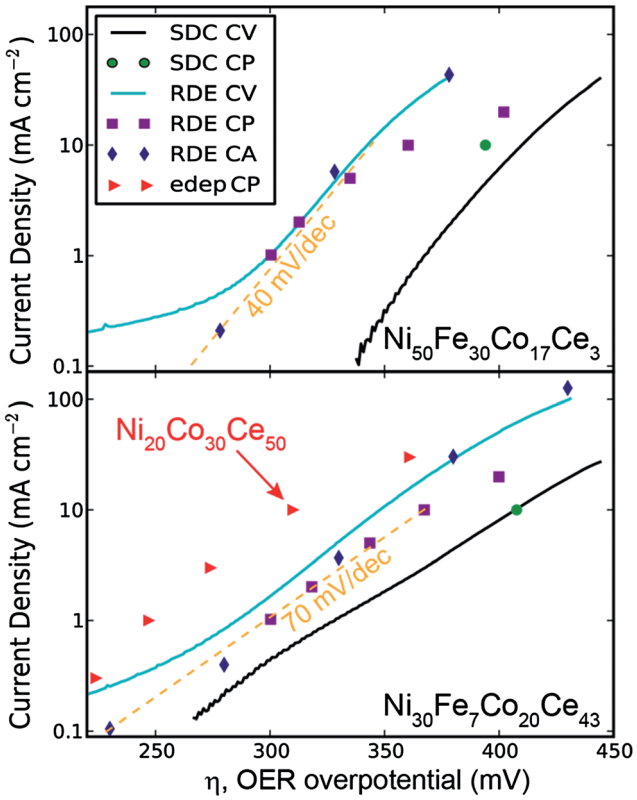

Fig. 3 Catalyst performance data for representative samples in the two composition regions of interest, (top) *low-Ce* and (bottom) *high-Ce*. The solid black curve is the CV and the green circle is the CP collected on the 1 mm^2 composition library sample. The blue curve, purple squares, and purple diamonds are the CV, CP, and CA data collected with 5 mm diameter glassy carbon rotating disk electrodes. The red triangles are the stabilized overpotentials measured from 90 second duration CP (at current densities 30, 10, 3, 1, 0.3 mA cm^{-2} geometric area) collected on the *high-Ce* ternary composition electrodeposited on a gold RDE. In each plot, the dashed orange line shows the representative Tafel slope between 0.1 and 10 mA cm^{-2}.

Using these data in the 0.1 to 10 mA cm^{-2} range, the Tafel slopes for the low-Ce and high-Ce catalysts were found to be approximately 40 mV dec^{-1} and 70 mV dec^{-1}, respectively. These slopes are shown in Fig. 3, and for each catalyst a similar Tafel slope is observed for both the SDC CV and RDE CV measurements. The low-Ce Tafel slope is similar to reported values between 30 and 45 mV dec^{-1} reported for $Fe_{0.1}Ni_{0.9}O_x$ to $Fe_{0.5}Ni_{0.5}O_x$.[1,10,12,13] We note that the measurements above 10 mA cm^{-2} have known artifacts due to bubble formation and adhesion onto the catalyst surface. Compared to the previously studied (Ni–Fe)O_x catalyst in the *low-Ce* composition region, the newly discovered *high-Ce* catalyst exhibited a significantly larger Tafel slope. The value of the Tafel slope is related to the fundamental reaction mechanism of catalysis, particularly for the rate limiting step.[1,29–31] However, more than one proposed reaction mechanism will produce the same Tafel slope, so the Tafel slope cannot be used as the sole diagnostic parameter for determining the reaction mechanism, particularly for a complex $4e^-$ reaction like the OER. However, observation of different Tafel slopes for the *low-Ce* and the *high-Ce* catalyst compositions is a strong indication that a change in reaction mechanism or rate limiting step has occurred.

The Tafel slope is also an important engineering parameter. In conventional electrolytic cells, a catalyst with a low Tafel slope is preferred, because these devices are operated at high geometric current densities, typically in excess of 1 A cm^{-2}. A low Tafel slope indicates that a large increase in the current density exacts a relatively small increase in applied overpotential. That is, the rate of production can be increased with only a small penalty in efficiency, or production cost. In distributed solar fuels generation the applicable current densities are far lower, near 10 mA cm^{-2}, and the focus of catalyst development is to minimize the overpotential at this current density. At these current densities, the effective exchange current density may be a more significant measure of catalyst suitability than the Tafel slope.[1] The Tafel slope also indicates the decrease in catalyst overpotential at a particular geometric current density that can be attained by an increase in surface area. For example, at a current density of 10 mA cm^{-2} creating a *low-Ce* catalyst with ten-fold increase in surface area would decrease the overpotential by approximately 40 mV. Making the same modification to the *high-Ce* catalyst would decrease the overpotential by approximately 70 mV.

The difference in current between the SDC and RDE data may be due not only to measurement conditions, such as resistance compensation and mass transport, but also to differences in sample morphology. The RDE-prepared samples may have larger specific surface areas, which in inkjet printing-based synthesis can be influenced by the substrate as well as the amount of catalyst deposited on the substrate. The electrochemical measurements indicated that the electrochemically accessible surface area derived from the CV capacitive current of each RDE sample was approximately ten times the planar area of the electrode. For the electrodeposited sample, the electrochemically accessible surface area was approximately five times the planar area, indicating that the increased catalytic current for this sample was not the result of increased surface area. The underlying cause of improved catalysis of the electrodeposited sample requires further investigation, but given the consistency of the Tafel slopes, we assert that the electrodeposition technique yielded a higher surface concentration of active electrochemical sites.

Select catalysts were characterized using bulk (energy dispersive X-ray spectroscopy, EDS) and near-surface (X-ray photoelectron spectroscopy, XPS) composition measurements (Table 1, and ESI†). The EDS analysis demonstrates the fidelity of the synthesis method, as the intended compositions are well within the uncertainty of the measured compositions. While the quantification of the XPS measurements is prone to systematic errors for this set of elements, these measurements provide important characterization of relative compositions. The relative near surface composition of the as-calcined *low-Ce* and *high-Ce* catalysts are commensurate with the change in the bulk composition.

Combined with electrochemical testing, the composition measurements also provide important characterization of catalyst stability. The stability of OER catalytic activity of the

Table 1 Comparison of intended film compositions inkjet-printed onto glassy carbon disks with those measured by EDS and XPS as-calcined and after the standard battery of electrochemical tests. The XPS analysis indicates that the surface composition may differ from the bulk

		EDS composition		XPS compositions	
Sample	Target composition	As-calcined	After e-chem	As-calcined	After e-chem
Low-Ce	$Ni_{50}Fe_{30}Co_{17}Ce_3$	$Ni_{54}Fe_{26}Co_{16}Ce_4$	$Ni_{58}Fe_{21}Co_{18}Ce_3$	$Ni_{71}Fe_{12}Co_{13}Ce_3$	$Ni_{73}Fe_{10}Co_{16}Ce_1$
High-Ce	$Ni_{30}Fe_7Co_{20}Ce_{43}$	$Ni_{34}Fe_7Co_{20}Ce_{39}$	$Ni_{32}Fe_6Co_{19}Ce_{43}$	$Ni_{48}Fe_2Co_{18}Ce_{32}$	$Ni_{49}Fe_2Co_{23}Ce_{26}$

low-Ce and *high-Ce* catalysts was evaluated using 2 h RDE CP measurement at 10 mA cm^{-2} during which the measured potential remained essentially unchanged. Composition measurements before and after the suite of RDE electrochemical experiments (Fig. 4) showed that the bulk and near-surface catalyst compositions remained largely unchanged by the extensive electrochemical testing (see Table 1). Considering the relative EDS and XPS measurements, the low-Ce catalyst may have lost some Fe but is overall quite electrochemically stable, and the high-Ce catalyst shows excellent electrochemical stability.

The *high-Ce* catalyst was also tested in a solar fuels testbed system in which an alkaline electrolyzer was built using an 11 μm-thick anion exchange membrane (Tokuyama A901), sputtered NiMo cathode, and $Ni_{0.3}Fe_{0.07}Co_{0.2}Ce_{0.43}O_x$ anode. The 2.5 cm^2 planar anode was prepared using the inkjet deposition method described above, creating a *high-Ce* catalyst similar to that contained in the catalyst library of Fig. 1. Powered by a triple junction Si photovoltaic under approximately AM1.5 illumination (15 cm^2 area, $V_{oc} = 2.0$ V, $J_{sc} = 5.5$ mA cm^{-2}, FF = 0.51), the electrolyzer maintained 3.5–4.5 mA cm^{-2} of hydrogen production over the 100 h experiment, demonstrating the stability of the catalyst under operating conditions. Following the 100 h stability test, the testbed system was operated in conjunction with a gas analysis system in which gasses were collected from the anode and cathode headspaces and measured to be O_2 and H_2, respectively. The gasses were produced in the expected 1 : 2 volume ratio and comparison with the measured current demonstrated faradaic efficiency in excess of 97% (see ESI†).

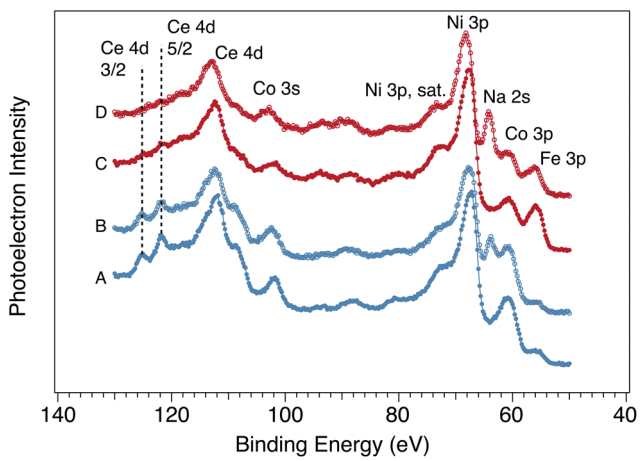

Fig. 4 High-resolution XPS spectra of the Ce4d, Ni3p, Co3p, and Fe3p region from the GC RDE samples. (A) *High-Ce* composition as-calcined at 350 °C and (B) after 2 h CP at 10 mA cm^{-2}. (C) *Low-Ce* composition as-calcined at 350 °C and (D) after 2 h CP at 10 mA cm^{-2}. The Na 2s peak only appears on samples exposed to 1.0 M NaOH during electrochemical testing.

Direct comparison with catalysts reported in the literature is confounded by the wide variety of electrochemical testing conditions and diverse performance metrics used in the literature. Many factors are known to impact the measured catalyst performance (overpotential at a particular current density), including the real surface area, the electrochemically active surface area, preconditioning to convert to an active form of the catalyst, composition of the substrate, pH, electrolyte, and specific absorption of buffering agents. In the search for mechanistic insights different researchers have not only used different measurement conditions, but have used different performance metrics (specific activity, several definitions of turnover frequency, or other metrics of their own devising). A detailed comparison of recently reported OER catalysts measured using disparate methods is beyond the scope of this communication. We refer the reader to just such a comparison by Trotochaud and Boettcher.[32]

We are most interested in the discovery of electrocatalysts technologically relevant to distributed photoelectrochemical fuels generation, which requires low overpotential at a current density of approximately 10 mA cm^{-2} geometric area. Fortunately, a protocol specific to standardized testing of electrocatalysts under conditions appropriate for distributed solar fuels generation has recently been developed and published.[21] This foundational report includes the electrodeposition, standardized electrochemical testing, and comparison to literature values of 10 metal oxide compositions. The most active catalysts and their initial overpotentials at 10 mA cm^{-2} were: IrO_x, 0.32 V; $NiFeO_x$, 0.35 V; $CoFeO_x$, 0.37 V; $NiCoO_x$, 0.38 V; $NiCeO_x$, 0.43 V. When subjected to identical electrochemical tests and conditions, the newly discovered *high-Ce* composition, inkjet-printed catalyst is among the most active of the earth-abundant OER catalysts (η = 0.37 V). When subjected to similar electrochemical tests and conditions, the electrochemically deposited pseudoternary *high-Ce* composition, $Ni_{0.2}Co_{0.3}Ce_{0.5}O_x$ produced an even lower overpotential ($\eta = 0.31$ V). The low overpotential produced by the electrodeposited catalyst may result from one or more potential factors, including microstructure (it was not calcined at 350 °C), substrate effects (gold substrate instead of glassy carbon), or greater hydroxide incorporation. The source of this greater activity requires further investigation, but is encouraging for the further improvement of this catalyst and

clearly demonstrates the validity of the activities of catalysts prepared by inkjet printing and calcination of precursors.

An alternative method of comparing activities among catalyst compositions is to simply compare the relative activity within our library, in which all compositions are prepared on the same substrate using the same methods, at the same metal-atom coverage, and then tested using identical conditions and methods. This particular library on FTO-coated glass contains binary $(Ni,Fe)O_x$ and $(Ni,Co)O_x$ compositions known to be among the most active for OER in basic conditions. Inspection of the maps of η at 10 mA cm^{-2} (see Fig. 1 and 2), indicate that both the *low-Ce* and the *high-Ce* catalyst compositions produce lower overpotential than either $Ni_{0.5}Fe_{0.5}O_x$ or $Ni_{0.5}Co_{0.5}O_x$. The library substrate and synthesis conditions are not intended to produce optimized microstructures or surface areas for OER catalysis; however, it is possible that the relative performance of the catalyst compositions will be retained with optimization. In particular, optimization of the structure and performance of the *high-Ce* composition to exploit its unique Tafel behavior requires further investigation and may yield a far superior catalyst.

The performance and stability data of Fig. 1–4 mark the discovery of a new family of OER catalysts with excellent performance in the current density and overpotential range applicable to artificial photosynthesis. This high activity has been retained for compositions synthesized by multiple synthetic methods on three different substrates. This new catalyst's high activity has been validated using a standardized electrochemical testing protocol, showing that it is among the most active OER catalysts under pH 14 conditions. Additional optimization of the structure of this catalyst is predicted to further decrease the operating overpotential at 10 mA cm^{-2}. This finding provides new research directions for OER catalysis and highlights the utility of high throughput methods for the discovery of energy related materials. The accelerated technology development surmounted a common challenge faced by high throughput discovery efforts. Connecting high throughput screening to validation experiments and to rapid incorporation into an operational device creates an unprecedented platform for material discovery.

Acknowledgements

This material is based upon work performed by the Joint Center for Artificial Photosynthesis, a DOE Energy Innovation Hub, supported through the Office of Science of the U.S. Department of Energy (Award no. DE-SC0004993). The authors thank Charles McCrory for assistance with acquisition, analysis and interpretation of traditional electrochemistry on rotating disc electrodes; Dan Guevarra for assistance with high throughput electrochemistry experiments; Paul Newhouse for assistance with preparation of glassy carbon rods for printing; William West and Chris Karp for assistance with electrolyzer testbed faradaic efficiency and headspace measurements; Martin Marcin for assistance with assembly of high throughput electrochemistry experiments; the Microanalytical Center in the College of Chemistry, UC Berkeley for ICP-OES measurements; Karl Walczak for preparation of the NiMo cathode used in the testbed system; and the U. S. Army Research Laboratory for providing the anion exchange membrane used in the testbed system.

References and Notes

1 M. G. Walter, E. L. Warren, J. R. McKone, S. W. Boettcher, Q. X. Mi, E. A. Santori and N. S. Lewis, *Chem. Rev.*, 2010, **110**, 6446–6473.
2 T. R. Cook, D. K. Dogutan, S. Y. Reece, Y. Surendranath, T. S. Teets and D. G. Nocera, *Chem. Rev.*, 2010, **110**, 6474–6502.
3 J. Suntivich, K. J. May, H. A. Gasteiger, J. B. Goodenough and Y. Shao-Horn, *Science*, 2011, **334**, 1383–1385.
4 M. Woodhouse and B. A. Parkinson, *Chem. Soc. Rev.*, 2009, **38**, 197–210.
5 G. Y. Chen, D. A. Delafuente, S. Sarangapani and T. E. Mallouk, *Catal. Today*, 2001, **67**, 341–355.
6 T. F. Jaramillo, A. Ivanovskaya and E. W. McFarland, *J. Comb. Chem.*, 2002, **4**, 17–22.
7 D. Seley, K. Ayers and B. A. Parkinson, *ACS Comb. Sci.*, 2013, **15**, 82–89.
8 J. B. Gerken, J. Y. C. Chen, R. C. Masse, A. B. Powell and S. S. Stahl, *Angew. Chem., Int. Ed.*, 2012, **51**, 6676–6680.
9 A. Minguzzi, M. A. Alpuche-Aviles, J. R. Lopez, S. Rondinini and A. J. Bard, *Anal. Chem.*, 2008, **80**, 4055–4064.
10 R. D. L. P. Smith, M. S. Prevot, R. D. Fagan, S. Trudel and C. P. Berlinquette, *J. Am. Chem. Soc.*, 2013, **135**, 11580–11586.
11 X. N. Liu, Y. Shen, R. T. Yang, S. H. Zou, X. L. Ji, L. Shi, Y. C. Zhang, D. Y. Liu, L. P. Xiao, X. M. Zheng, S. Li, J. Fan and G. D. Stucky, *Nano Lett.*, 2012, **12**, 5733–5739.
12 L. Trotochaud, J. K. Ranney, K. N. Williams and S. W. Boettcher, *J. Am. Chem. Soc.*, 2012, **134**, 17253–17261.
13 M. W. Louie and A. T. Bell, *J. Am. Chem. Soc.*, 2013, **135**, 12329–12337.
14 D. A. Corrigan, *J. Electrochem. Soc.*, 1987, **134**, 377–384.
15 I. Nikolov, R. Darkaoui, E. Zhecheva, R. Stoyanova, N. Dimitrov and T. Vitanov, *J. Electroanal. Chem.*, 1997, **429**, 157–168.
16 E. B. Castro and C. A. Gervasi, *Int. J. Hydrogen Energy*, 2000, **25**, 1163–1170.
17 E. B. Castro, S. G. Real and L. F. P. Dick, *Int. J. Hydrogen Energy*, 2004, **29**, 255–261.
18 S. K. Tiwari, S. Samuel, R. N. Singh, G. Poillerat, J. F. Koenig and P. Chartier, *Int. J. Hydrogen Energy*, 1995, **20**, 9–15.
19 C. Bocca, A. Barbucci, M. Delucchi and G. Cerisola, *Int. J. Hydrogen Energy*, 1999, **24**, 21–26.
20 D. A. Corrigan and R. M. Bendert, *J. Electroanal. Chem.*, 1989, **136**, 723–728.
21 C. C. L. McCrory, S. Jung, J. C. Peters and T. F. Jaramillo, *J. Am. Chem. Soc.*, 2013, **135**, 16977–16987.
22 J. M. Gregoire, C. Xiang, S. Mitrovic, X. Liu, M. Marcin, E. W. Cornell, J. Fan and J. Jin, *J. Electrochem. Soc.*, 2013, **160**, F337–F342.
23 J. M. Gregoire, C. X. Xiang, X. N. Liu, M. Marcin and J. Jin, *Rev. Sci. Instrum.*, 2013, **84**, 024102.
24 J. Fan, S. W. Boettcher and G. D. Stucky, *Chem. Mater.*, 2006, **18**, 6391–6396.

25 R. D. L. Smith, M. S. Prevot, R. D. Fagan, Z. P. Zhang, P. A. Sedach, M. K. J. Siu, S. Trudel and C. P. Berlinguette, *Science*, 2013, **340**, 60–63.
26 K. J. May, C. E. Carlton, K. A. Stoerzinger, M. Risch, J. Suntivich, Y. L. Lee, A. Grimaud and Y. Shao-Horn, *J. Phys. Chem. Lett.*, 2012, **3**, 3264–3270.
27 Y. Gorlin and T. F. Jaramillo, *J. Am. Chem. Soc.*, 2010, **132**, 13612–13614.
28 Y. Matsumoto and E. Sato, *Mater. Chem. Phys.*, 1986, **14**, 397–426.
29 A. J. Bard and L. R. Faulkner, *Electrochemical Methods*, John Wiley & Sons, Inc, 2001.
30 J. O. Bockris, *J. Chem. Phys.*, 1956, **24**, 817–827.
31 J. O. Bockris and T. Otagawa, *J. Phys. Chem.*, 1983, **87**, 2960–2971.
32 L. Trotochaud and S. W. Boettcher, *Scr. Mater.*, 2014, **74**, 25–32.